


Article

Utilizing Recycled Expanded Polystyrene Plastics to Stabilize Metal–Organic Frameworks for Heterogeneous Catalysis

Ruizhi Yin ¹, Enxi Shen ¹, Chenjia Liang ¹, Dezhong Song ¹, Samir El Hankari ² and Jia Huo ^{1,3,*}

¹ College of Chemistry and Chemical Engineering, Hunan University, Changsha 410082, China; rui0110@hnu.edu.cn (R.Y.); exshen0606@163.com (E.S.); cjiang01123@163.com (C.L.); dzsong@hnu.edu.cn (D.S.)

² Chemical and Biochemical Sciences, Green Process Engineering, Mohammed VI Polytechnic 6 University (UM6P), Lot 660—Hay Moulay Rachid, Ben Guerir 43150, Morocco; elhankarisamir@gmail.com

³ Greater Bay Area Institute for Innovation, Hunan University, Guangzhou 511300, China

* Correspondence: jiahuo@hnu.edu.cn

Abstract: Polystyrene plastics present significant environmental and human health threats due to their poor recyclability and degradability. However, leveraging their properties to enhance material performance stands out as one of the most effective strategies for mitigating these issues. Here, we have employed recycled expanded polystyrene plastics to manufacture metal–organic framework/expanded polystyrene plastic composites (MOF@EPP) using an adverse solvent precipitation method. This method simultaneously recycles EPPs and safeguards moisture-sensitive MOFs. Due to the exceptional hydrophobic properties of EPPs, HKUST–1@EPP can maintain structural integrity even when immersed in water for 30 days. This method is applicable to other moisture-sensitive MOFs, such as MOF–74(Zn) and MIL–53(Al). The HKUST–1@EPP composite also exhibits desirable heterogeneous catalytic activity in the Knoevenagel condensation reaction between benzaldehyde and acrylonitrile. The conversion rate can reach 94.9% within 4 h at 90 °C and does not exhibit a significant decrease even after six cycles, even in the presence of water. This study not only introduces a novel concept for recycling polystyrene plastics, but also offers a practical strategy for safeguarding moisture-sensitive MOFs.

Keywords: metal–organic frameworks; recycling polystyrene plastics; water stability; heterogeneous catalysis



Citation: Yin, R.; Shen, E.; Liang, C.; Song, D.; El Hankari, S.; Huo, J. Utilizing Recycled Expanded Polystyrene Plastics to Stabilize Metal–Organic Frameworks for Heterogeneous Catalysis. *Processes* **2024**, *12*, 961. <https://doi.org/10.3390/pr12050961>

Academic Editor: Chenxi Zhang

Received: 17 April 2024

Revised: 2 May 2024

Accepted: 6 May 2024

Published: 9 May 2024



Copyright: © 2024 by the authors. Licensee MDPI, Basel, Switzerland. This article is an open access article distributed under the terms and conditions of the Creative Commons Attribution (CC BY) license (<https://creativecommons.org/licenses/by/4.0/>).

1. Introduction

The rapid growth of modern industry has led to a surge in polystyrene plastic packaging, yet inadequate management practices have resulted in severe global environmental repercussions [1–5]. According to the United Nations Environment Programme, single-use plastics and polystyrene foam are consistently among the top ten contributors to marine pollution, with over eight million tons of plastic entering the oceans annually [6–8]. The detrimental plastic waste, such as that in the form of small or microplastic debris, has a heightened probability of permeating food chains, thereby posing potential threats to ecologically significant species such as mussels, salt-marsh grasses, and fishes. Both humans and mussels that ingest these small or microplastic debris may experience accumulation within their bodies, leading to cellular and tissue harm [1]. Due to the inherent difficulty in handling polystyrene plastic, recycling emerges as a crucial method for mitigating this environmental strain, typically employing mechanical, biological, chemical, and thermal processes, which are complex and resource-intensive [9,10]. Therefore, an alternative approach involving the production of high-value materials from polystyrene waste offers a potential solution to both environmental protection and economic enhancement [11].

Metal–organic frameworks (MOFs) represent a highly promising class of multifunctional porous materials, comprising metal ions/cluster centers and multivalent organic

linkers [12–16]. Owing to their exceptionally high surface areas (typically ranging from 1000 to 10,000 m² g^{−1}), tunable pore sizes, diverse structures, and abundant active sites [17,18], MOFs exhibit remarkable versatility for various applications, including guest storage, gas/pollutant separation [19–22], heterogeneous catalysis, photocatalysis, sensing, and biomedicine [23–30]. Although MOFs exhibit potential applications in various fields, their stability is recognized as a significant barrier hindering practical utilization. Most MOFs are susceptible to disruption by strong coordination in water or even under an ambient atmospheric environment because of the weak and dynamic coordination between metal ions and organic ligands, such as MOF–5, HKUST–1, etc. [31,32]. Therefore, despite thousands of papers being published each year, there are hardly any examples of MOFs being widely applied in industry [33–35].

To address the challenges of instability and expand the practical utility of existing MOFs, researchers have recently pursued three primary strategies [29]. The first approach involves constructing MOFs with strong coordination bonds, such as Zr(Hf)–O and Cr–O. UiO–66, formed with Zr–O bonds, is one of the most stable MOFs, even in strongly acidic or alkaline solutions [14]. This approach is only limited to a few MOFs, such as UiO–66 and MIL–101, and the stability of formed MOFs is often affected by the functional groups in the organic linkers. The second is functionalizing unstable MOFs with hydrophobic organic linkers [36–39]. For instance, Cohen et al. introduced hydrophobic alkyl groups to the ligands of MOFs. This functionalization resulted in the enhanced hydrolytic stability of IRMOF–3, which could retain the original crystal structure even after being placed in water for 30 min; however, the nonfunctionalized MOFs immediately changed in structure when in contact with the water [38]. However, this approach often leads to a significant reduction in porosity and adsorption properties, due to the occupation of channels by dangling functional groups [19]. Another approach entails modifying the outer surface of MOFs by incorporating hydrophobic layers [40–42], such as carboxy-functionalized attapulgite groups, polydimethylsiloxane coating [42], and even polydopamine [31]. While these methods have improved the stability of certain MOFs, their complex and costly nature limits their scalability and widespread adoption.

Building on this premise, we have devised a cost-effective and user-friendly approach to enhance the hydrothermal stability of conventional moisture-sensitive MOFs while preserving their functionality, such as their catalytic activity. Specifically, we synthesized metal–organic framework/expanded polystyrene plastic composites (MOF@EPP) utilizing polystyrene plastic waste through an adverse solvent precipitation method. The hydrophobic nature of polystyrene plastics leads to a notable enhancement in the stability of MOFs within aqueous environments, even for 30 days. This method can be widely applied to different moisture-sensitive MOFs, such as HKUST–1, MOF–74(Zn), and MIL–53(Al). The HKUST–1@EPP composite also exhibits excellent heterogeneous catalytic activity in the Knoevenagel condensation reaction between benzaldehyde and acrylonitrile. The conversion rate can reach 94.9% within 4 h at 90 °C and does not exhibit a significant decrease even after six cycles, even in the presence of water. This method offers a novel avenue for simultaneous plastic recycling and safeguarding moisture-sensitive MOFs.

2. Materials and Methods

2.1. Materials

Copper acetate monohydrate, lauric acid, and 1,3,5-benzenetricarboxylic acid were procured from Aladdin Reagent Company, Los Angeles, CA, USA. Aluminum nitrate hydrate, zinc nitrate hexahydrate, and chloroform were obtained from Shanghai National Pharmaceutical Reagent Company, Shanghai, China. Methanol, ethanol, n-butanol, and N,N-dimethylformamide (DMF) were sourced from Shanghai Titan Technology Co., Shanghai, China. Terephthalic acid was acquired from Wokai Reagent Co., Weinan, China, and 2,5-dihydroxyterephthalic acid was obtained from Energy Reagent Co., Shanghai, China. Triethylamine (TEA) was purchased from Xilong Reagent Company, Shantou, China. Expanded polystyrene plastic was recycled from packing foams.

2.2. Preparation of HKUST-1

The HKUST-1 was synthesized via a microwave heating process. Initially, 0.27 g (1.37 mmol) of $\text{Cu}(\text{CH}_3\text{COO})_2 \cdot \text{H}_2\text{O}$ and 8.76 g (43.75 mmol) of lauric acid were completely dissolved in 20 mL of n-butanol using ultrasonic waves, while 0.18 g (0.88 mmol) of 1,3,5-benzenetricarboxylic acid was dissolved in 5 mL of n-butanol. Subsequently, the solutions were combined in a 35-mL microwave reactor and heated to 140 °C at 150 W, which was maintained for 10 min, and then cooled to room temperature. The resulting solution was centrifuged at 8000 rpm for 5 min, and the supernatant was decanted to obtain a blue solid, which underwent washing with ethanol five times and drying under vacuum at 65 °C [42].

2.3. Preparation of MIL-53(Al)

The MIL-53(Al) was synthesized using a hydrothermal method. Initially, 1.37 g (8.25 mmol) of terephthalic acid and 11.74 g (16.50 mmol) of $\text{Al}(\text{NO}_3)_3 \cdot 9\text{H}_2\text{O}$ were dissolved in 25 mL of DMF and stirred for 30 min. The resulting solution was then transferred into a flask and heated to 85 °C, with a ramping period of 4 h, followed by a reaction time of 20 h. The stirring at 240 rpm was maintained throughout the process using a magnetic stirrer. Subsequently, the flask was cooled to room temperature over the course of 30 min. The resulting precipitates were centrifuged and washed with ethanol five times before being dried under vacuum at 65 °C [43].

2.4. Preparation of MOF-74(Zn)

The MOF-74(Zn) was synthesized via room-temperature precipitation. Initially, 0.081 g (0.41 mmol) of 2,5-dihydroxyterephthalic acid and 0.19 g (0.64 mmol) of $\text{Zn}(\text{NO}_3)_2 \cdot 6\text{H}_2\text{O}$ were dissolved in a solution comprising 5 mL of DMF, 600 µL of ethanol, and 600 µL of deionized water. The solution underwent ultrasonic mixing and was subsequently stirred magnetically at room temperature, during which 300 µL of TEA was added dropwise over the course of 1 min. The reaction was allowed to proceed for an additional hour with stirring. The resulting precipitates were washed and centrifuged with DMF and ethanol, five times each, followed by drying under vacuum at 65 °C [44].

2.5. Preparation of HKUST-1@EPP

A total of 0.15 g of HKUST-1 nanoparticles were dispersed in 2 mL of chloroform solvent using ultrasonic waves, while 1.35 g of packaging foam was crushed and dispersed in 3 mL of chloroform solvent. Subsequently, the two dispersions were combined. Approximately 0.40 mL of the dispersible liquid was drawn into a 1-mL syringe and then dripped into a 20-mL methanol solution, resulting in the formation of 1–5-mm blue spherical particles. The HKUST-1@EPP particles were obtained by drying under vacuum at 65 °C.

2.6. Preparation of MIL-53(Al)@EPP

A total of 0.15 g of MIL-53(Al) nanoparticles were dispersed in 2 mL of DMF using ultrasonic waves, while 1.5 g of packaging foam was crushed and dispersed in 2 mL of DMF solvent. Subsequently, the two dispersions were combined. Approximately 0.40 mL of the dispersible liquid was drawn into a 1-mL syringe and then dripped into a 20-mL methanol solution, resulting in the formation of 2–6-mm blue spherical particles. The MIL-53(Al)@EPP particles were obtained by drying under vacuum at 65 °C.

2.7. Preparation of MOF-74(Zn)@EPP

A total of 0.12 g of MOF-74(Zn) nanoparticles were dispersed in 2 mL of acetone using ultrasonic waves, while 1.5 g of packaging foam was crushed and dispersed in 3 mL of chloroform solvent. Subsequently, the two dispersions were combined. Approximately 0.40 mL of the dispersible liquid was drawn into a 1-mL syringe and then dripped into a 20-mL methanol solution, resulting in the formation of 3–5-mm blue spherical particles. The MOF-74(Zn)@EPP particles were obtained by drying under vacuum at 65 °C.

2.8. Characterization Method Section

The phase identification of the samples was performed on a Powder X-ray diffractometer (PXRD, D8 Advance, Shanghai Fuzhan Environmental Protection Technology Co., Ltd., Shanghai, China) using Cu K α radiation, where the scanning range of the diffraction angle (2-Theta) was 5–50°. The scanning rate was 4° min^{−1} and the step width was 0.02°, with 40-mA operation current and 40-kV voltage. The thermogravimetric analysis (TGA) was performed using an HTG-1 (HENVEN) instrument (Beijing HENVEN Experimental Equipment Co., Ltd., Beijing, China), and the sample was heated from room temperature to 800 °C at a rate of 10 °C min^{−1} under a N₂ atmosphere. The scanning electron microscopy (SEM) measurements were made on a Hitachi S-4800 (Qingdao Jiading Analytical Instrument Co., Ltd., Qingdao, China) field emission scanning electron microscope at an accelerating voltage of 5, 10, or 15 kV. The samples for the SEM measurements were attached to the stub using carbon paste and then sputter-coated with a thin layer of conductive gold to improve their electrical conductivity. The nitrogen adsorption–desorption isotherms were measured at 77 K with a JW-BK200C (Beijing Jingweigaobo Science and Technology Co., Ltd., Beijing, China) gas adsorption analyzer after the sample was first degassed at 120 °C overnight. The specific surface areas were determined using the BET method, the mesopore size distribution was obtained based on BJH analysis of the desorption branches of the isotherms, and the total pore volumes were determined using the desorption branch of the N₂ isotherm at $p/p^0 = 0.99$ (single point). The gas chromatographic (GC) analysis was performed using an instrument model sp-7820 instrument (Shandong Lunan Ruihong Chemical Instrument Co., Ltd., Jinan, China) equipped with a flame ionization detector (FID) and an SE-54 column (length = 30 m, inner diameter = 0.32 mm, and film thickness = 0.50 μ m). The temperature for GC analysis was ramped from 60 to 140 °C at 20 °C min^{−1} and was held at 140 °C for 1 min. Then, it was heated from 140 to 142 at 1 °C min^{−1}; was ramped to 280 °C at 20 °C min^{−1}; and was then held at 280 °C for 2 min. The inlet and detector temperatures were set at 280 °C. n-Dodecane was used as an internal standard to calculate reaction conversion. The liquid products were also analyzed and quantified through a Bruker 400 MHz (AVANCE) NMR spectroscope (Bruker (Beijing) Technology Co., Ltd., Beijing, China). After the reaction, 0.3 mL of solution was collected and mixed with CDCl₃ (0.5 mL) in an NMR tube for characterization.

2.9. Stability and Catalytic Experiment

The stability test was carried out via the following procedures: first, either MOF nanoparticles or MOFs@EPP particles were immersed in 50 mL of water for a specifically defined time (12 h, 1 d, 2 d, 3 d, 5 d, 10 d, 30 d); then, the MOF nanoparticles or MOFs@EPP particles were separated and dried under vacuum; finally, the structural changes in the MOF nanoparticles or MOFs@EPP particles were assessed using characterization methods such as PXRD.

For the catalytic experiment, 0.13 g (2 mmol) of malononitrile, 0.21 mL (2.1 mmol) of benzaldehyde, 0.1 mL of H₂O, and 100 mg of HKUST–1@EPP (or 10 mg of HKUST–1) were added to 20 mL of ethanol, followed by heating at 90 °C for a defined time. At a defined interval, a small amount of liquid containing the products was taken out using a syringe and was analyzed using GC and ¹H-NMR.

For the recycling experiment, after the reaction, the resultant catalysts were separated with a centrifuge, washed with ethanol, and dried under vacuum at 65 °C for reuse in a new reaction under the same conditions as the initial one. The recycling experiment was repeated 6 times.

3. Results

3.1. Synthesis and Characterization of Composites

Cu₃(BTC)₂ (BTC = benzene-1,3,5-tricarboxylate), also known as HKUST–1, is widely employed for gas adsorption and catalysis, owing to its highly porous structure, straightforward synthesis, and abundant coordinatively unsaturated sites [45–48]. Therefore, the

widespread application of HKUST-1 under practical environments is very important. However, normally, the exposure of HKUST-1 to humid conditions would prompt strong H_2O -Cu coordination, replacing the carboxylate bonds of BTC ligands from the Cu cluster, thus causing structural damage to HKUST-1. Recognizing this instability, we chose HKUST-1 as the initial model to illustrate the effective stabilization of metal-organic frameworks by incorporating a hydrophobic protective layer using recycled polystyrene. The HKUST-1@EPP was prepared by dropping a mixture of polystyrene and HKUST-1 nanoparticles in CHCl_3 into the immiscible solvent, methanol. The precipitate was collected by separation, washing in ethanol, and drying under vacuum. The preparation procedure is illustrated in Figure 1 (see the details in Section 2).

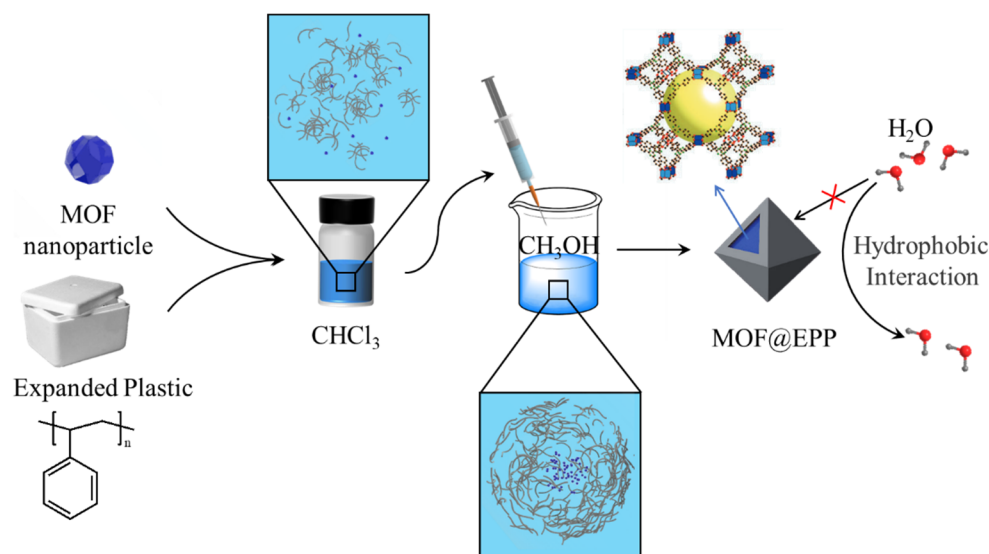


Figure 1. Illustration for the preparation procedure of MOF@EPP.

The morphology of the as-prepared materials was characterized with SEM. The SEM images of HKUST-1@EPP are depicted in Figure 2a, revealing that HKUST-1@EPP nanoparticles are displayed as relatively dense microspheres, with a diameter of approximately 1.7 μm . The formation of well-defined microspheres is reasonable by the consideration of the strong incompatibility between polystyrenes and methanol. The dense polystyrene would serve as a potential protective layer to stabilize HKUST-1. A cross-sectional SEM image demonstrates that the composites consist of numerous macropores with a diameter of around 200 μm , within which the HKUST-1 nanoparticles are encapsulated (Figure 2b). These macropores would facilitate guest diffusion during catalytic reactions. Furthermore, compared to the original HKUST-1 nanoparticles (Figure 3a), the size and morphology of HKUST-1 within the composites remains unchanged, confirming the desirable stability of HKUST-1 during the process. The components of HKUST-1@EPP were characterized using FTIR, along with those of HKUST-1 and expanded polystyrene plastics, as shown in Figure 2c. The carboxylate groups of HKUST-1 are evident from 1700 to 1500 cm^{-1} , corresponding to asymmetric and symmetric stretching vibrations. Compared to pristine HKUST-1, the FTIR spectrum of HKUST-1@EPP exhibits new peaks between 2700 and 3100 cm^{-1} , attributed to the aromatic ring C-H stretching vibration; peaks between 1575 and 1600 cm^{-1} , resulting from aromatic ring C=C stretching vibration on the benzene ring; peaks between 1445 and 1495 cm^{-1} , from the vibration mode on the aromatic ring; and peaks between 690 and 699 cm^{-1} , because of the out-of-plane vibration of the aromatic ring skeleton. This confirms that HKUST-1 nanoparticles were wrapped with polystyrenes.

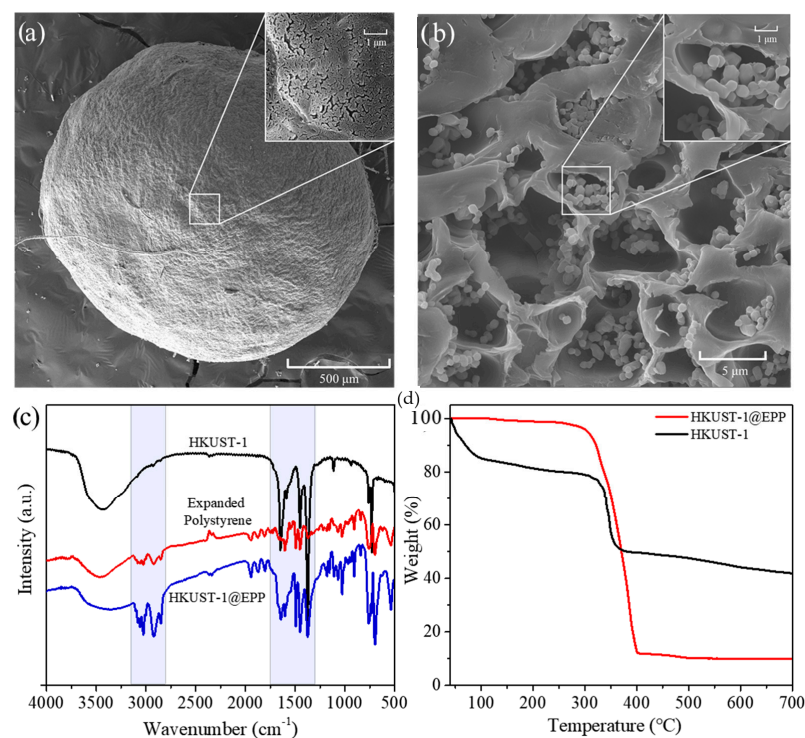


Figure 2. (a) SEM image of HKUST-1@EPP; (b) Cross-section SEM image of HKUST-1@EPP; (c) IR spectra of HKUST-1, expanded polystyrene and HKUST-1@EPP; and (d) TGA curves of HKUST-1 and HKUST-1@EPP.

TGA is instrumental in assessing the thermal stability of composites. The TGA curve of HKUST-1@EPP under a N_2 atmosphere is depicted in Figure 2d. It is shown that the weight reduction in the HKUST-1 nanoparticles commences at approximately 40 °C, primarily due to moisture absorption from the ambient air. Subsequently, there is a gradual decrease in the weight attributed to both physically and chemically adsorbed water within the skeletal structure, occurring within the temperature range of 100–320 °C, until the complete degradation of the HKUST-1 between 320 and 350 °C. Interestingly, in contrast to the rapid weight decrease in the pristine HKUST-1 nanoparticles, the TGA curve of HKUST-1@EPP shows that almost no obvious weight reduction is observed until 300 °C. This implies that almost no water was adsorbed into the composites, even though the sample was stored under the same conditions as the pristine HKUST-1 nanoparticles. The reduced water content in HKUST-1@EPP can be ascribed to the presence of a hydrophobic polystyrene protective shell, which effectively impedes water absorption by the HKUST-1 nanoparticles. Consequently, this underscores the hydrophobic nature and markedly enhanced water stability of HKUST-1@EPP, suggesting its superior performance over conventional HKUST-1 in practical applications.

The crystal structure of HKUST-1@EPP was characterized with PXRD. As shown in Figure 4a, a series of diffraction peaks at $2\theta = 6.8, 9.7, 11.8, 19.3,$ and 26.1° can be observed that match well with those of the simulated and as-prepared HKUST-1, and no other impurity was present, except for the broad peak at $2\theta = 20^\circ$, resulting from the amorphous polystyrene component. These results confirm the successful incorporation of HKUST-1 within the polystyrene matrixes, and the HKUST-1 nanoparticles still retained their original crystal structure. The porosity and specific surface area of HKUST-1@EPP can be analyzed from its N_2 isotherm, as shown in Figure 4b. The HKUST-1@EPP composite largely displays a type I isotherm, which is similar to that of the HKUST-1 nanoparticles. The specific surface area (calculated according to the BET method) of HKUST-1@EPP was calculated as $149 \text{ m}^2 \text{ g}^{-1}$, which is less than that of pristine HKUST-1 nanoparticles ($1387 \text{ m}^2 \text{ g}^{-1}$). The reduction can be mainly attributed to the presence of a large number

of polystyrenes (~90 wt%), which is consistent with the theoretical weight percentage of HKUST-1 in the composites (~10 wt%). The pore size distribution of HKUST-1@EPP is also similar to that of the pristine HKUST-1 nanoparticles (Figures S1 and S2). The porosity and surface area data show that the inner surfaces of HKUST-1 nanoparticles are still accessible after they have been encapsulated in the polystyrene matrixes, which would provide reaction zones for future heterogeneous catalysis.

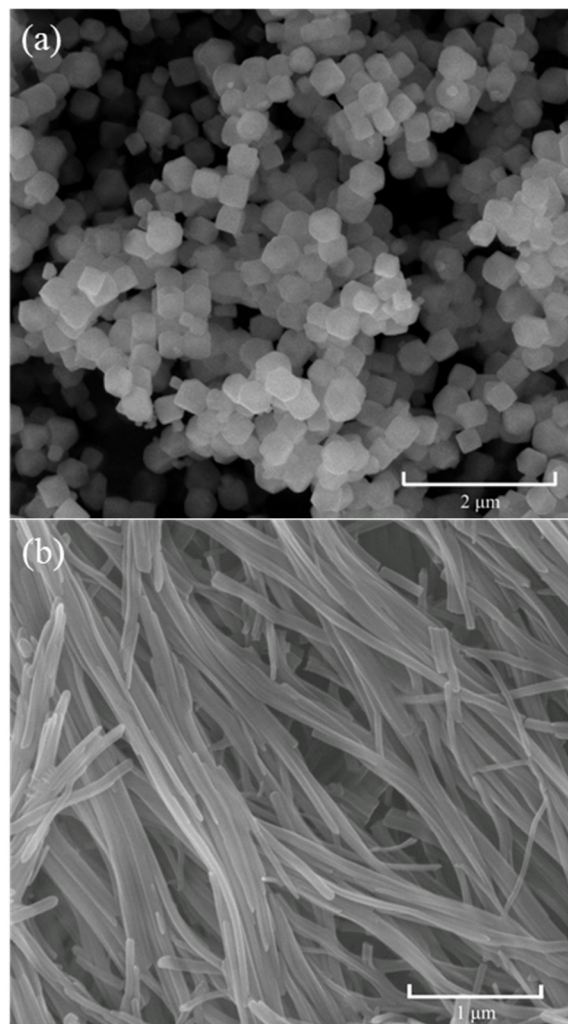


Figure 3. SEM images of HKUST-1 nanoparticles before (a) and after (b) immersion in water for 12 h.

Furthermore, the HKUST-1@EPP was directly immersed in water for different amounts of time to determine its water stability, with the pristine HKUST-1 nanoparticles being used as the control sample. The water stability of the HKUST-1 nanoparticles and HKUST-1 within the composites was evaluated using SEM and PXRD. The water stability of the HKUST-1 nanoparticles was first accessed. As shown in Figure 3, the SEM image of the pristine HKUST-1 nanoparticles shows that the nanoparticles are present as a well-formed polyhedron shape, with a diameter of ~200 nm. However, after the HKUST-1 nanoparticles were immersed in water for 12 h, the particles were completely changed into nanoneedles, which indicates that the structure of HKUST-1 was already destroyed because of the water. In order to further demonstrate the structure change in HKUST-1 after immersion in water, the samples were characterized with PXRD. As illustrated in the PXRD patterns in Figure 5a, after 12 h of immersion in water, the main characteristic peaks of HKUST-1 at 6.8, 9.7, and 11.8° vanish, and many new peaks around 10° and 23°

emerge, indicating that the crystal structure of the HKUST-1 nanoparticles was completely changed. This phenomenon was also observed by Pérez-Ramírez's group [49,50], who also found that the structure of HKUST-1 changes once exposed to water, suggesting the serious moisture instability of HKUST-1. As previously noted [49], exposure to water renders the crystal structure of HKUST-1 unstable, with rapid degradation occurring upon direct contact with liquid water. Notably, the PXRD analysis did not detect any traces of $\text{Cu}(\text{OH})_2$ or BTC ligands, suggesting that the degradation of the HKUST-1 crystal structure did not entail a complete collapse of the framework, as elegantly demonstrated by Pérez-Ramírez [50].

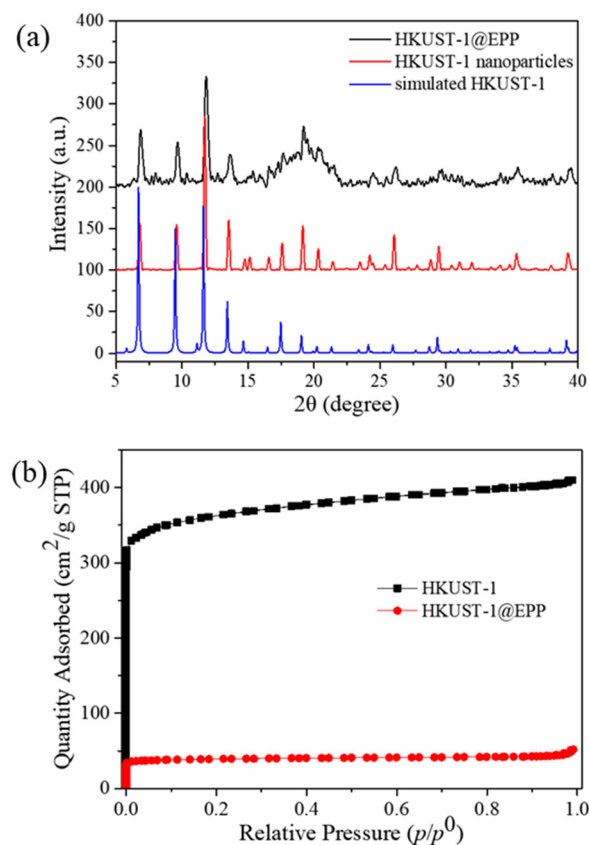


Figure 4. (a) PXRD patterns of simulated HKUST-1, HKUST-1 nanoparticles, and the HKUST-1@EPP; and (b) N_2 sorption/desorption isotherms of HKUST-1 nanoparticles and the HKUST-1@EPP.

After being encapsulated into the recycled polystyrene plastics, it was found that the water stability was significantly enhanced. Figure 5b shows the PXRD patterns of HKUST-1@EPP before and after several days of water immersion, which match well with that of HKUST-1; moreover, the principal diffraction peaks at 6.8° , 9.6° , 11.7° , 13.5° , and 19.2° for HKUST-1 are still observed in the patterns of the composites (Figures 3 and S2). Previously, the moisture stability was often carried under different humidity atmospheres. However, even when they were immersed in water for 30 days, all of the diffraction peaks of the HUST-1@EPP could be observed, which is indicative of the excellent water stability of the HKUST-1 in the composites. Additionally, a broad diffraction peak ranging from 15° to 25° can be attributed to the presence of amorphous polystyrene [51]. Based on the analysis of these PXRD patterns, the results indicate that the structure of HKUST-1@EPP remained largely unchanged after long-term water immersion, which was achieved by enveloping the HKUST-1 nanoparticles with polyethylene, significantly enhancing the water stability of HKUST-1.

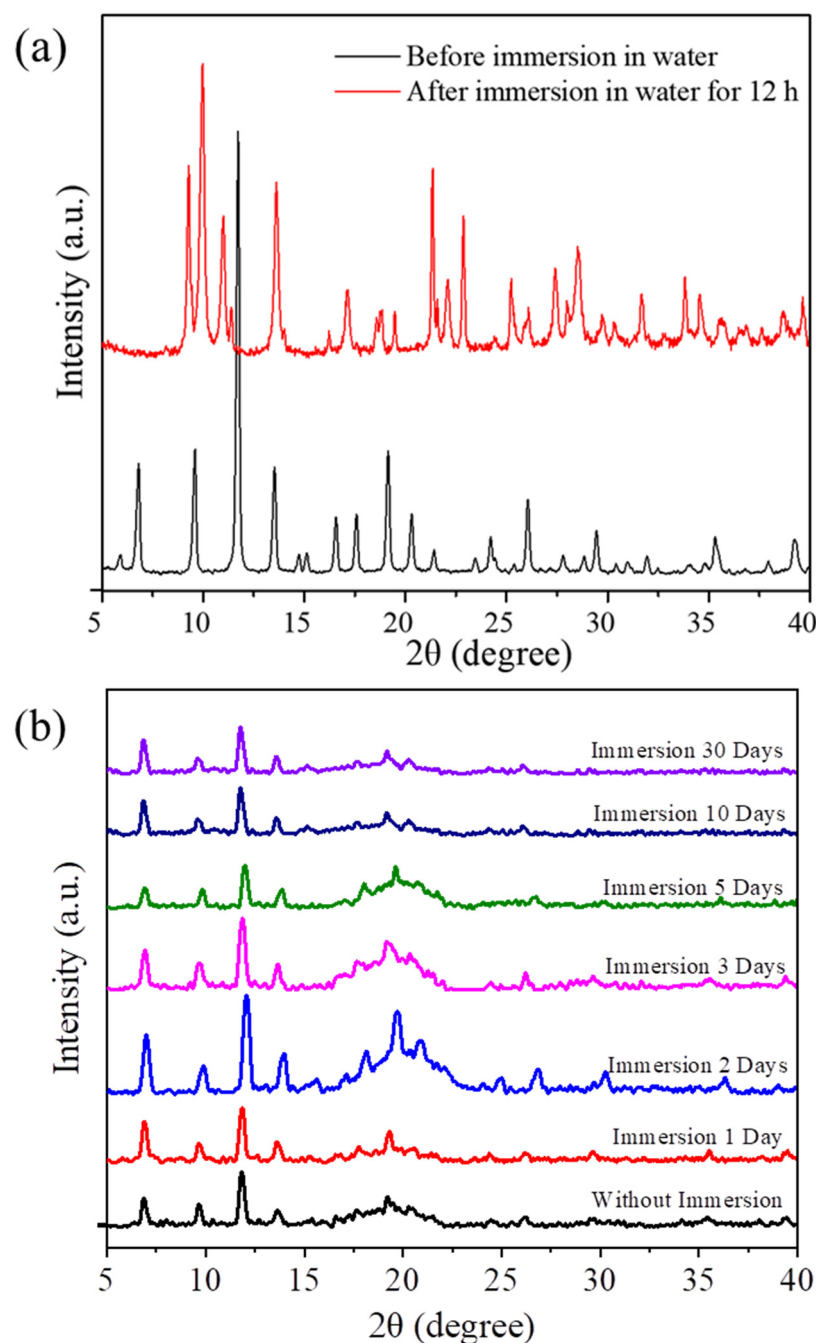


Figure 5. PXRD patterns of HKUST-1 nanoparticles (a) and HKUST-1@EPP (b) before and after water immersion stability test.

To illustrate the broad applicability and protective nature of this strategy beyond HKUST-1, MIL-53(Al) and MOF-74(Zn) were chosen for water immersion experiments. As depicted in Figure 6a, the structure of MOF-74(Zn)@EPP remains intact following a two-day immersion in water, without any discernible deviation in the major diffraction peaks at 6.7° and 11.8° , aligning with the PXRD pattern of pristine MOF-74(Zn) (Figure S3). Similarly, the significant diffraction peaks at 9.3° and 10.5° persist after subjecting MIL-53(Al)@EPP to the same immersion conditions for two days, as illustrated in Figure 6b. Notably, in comparison with the PXRD pattern of the simulated MIL-53(Al) in Figure S4, a broad diffraction peak spanning from 15° to 25° is the characteristic peak at 16.8° , which can be ascribed to the amorphous polystyrene. Based on the foregoing observations, it is deduced that the hydrophobic nature of MOF composites can result in HKUST-1

remaining largely unaffected, even after immersion in water for at least two days, affirming the efficacy and universality of this straightforward and environmentally friendly approach to enhancing the water stability of MOFs.

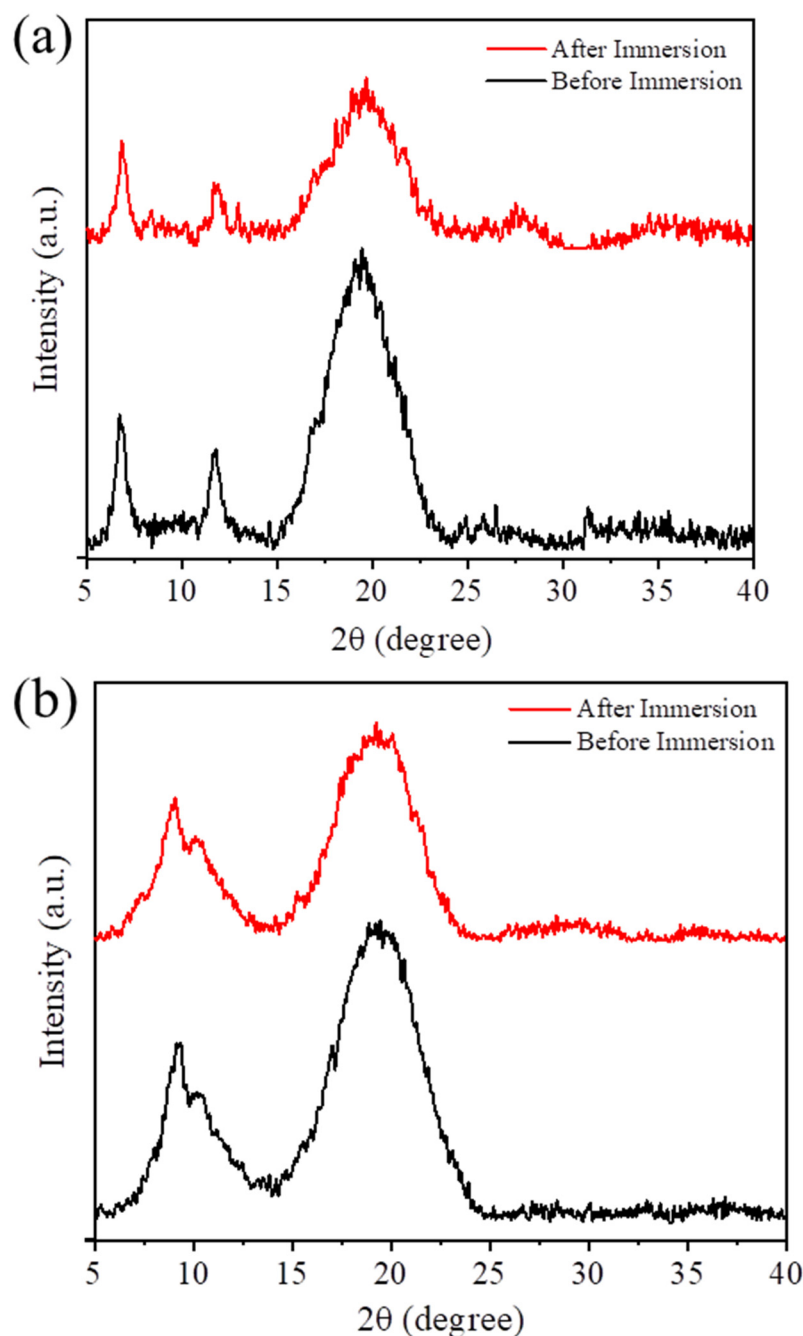


Figure 6. PXRD patterns of MOF-74(Zn)@EPP (a) and MIL-53(Al)@EPP (b) before and after water immersion test.

3.2. Catalytic Performance of Composites

The superior water stability of the MOF@EPP encouraged us to further underscore the potential applications of the MOF@EPP. Therefore, we further evaluated their performance in the Knoevenagel condensation reaction. This reaction, renowned for its versatility and significance, facilitates the formation of carbon-carbon double bonds [52,53] through the addition of aldehydes/ketones to active methylene hydrogen compounds [54]. In this work, we tested the catalytic activity of the HKUST-1@EPP to convert malononitrile and

benzaldehyde into benzylidene malononitrile (Figure 7a), an industrially and pharmaceutically significant product. To demonstrate the water stability, we added some water into the initial reaction mixture. As depicted in Figure 7b, the catalytic conversion of the HKUST-1@EPP to benzylidene malononitrile reached 94.9% after 4 h at 90 °C, surpassing that of HKUST-1 (87.2%). The desirable catalytic activity of HKUST-1@EPP confirms that the catalytic sites in the composites are still active even when they are encapsulated in the polystyrene matrixes. This enhancement is likely attributable to the hydrophobic nature of the HKUST-1@EPP, which minimizes water absorption by the encapsulated HKUST-1, thereby preventing structural collapse and facilitating the rapid departure of water molecules from the catalyst's active sites. Consequently, the overall reaction proceeds more efficiently, yielding higher conversion rates. Although the reaction rate of the HKUST-1@EPP is marginally lower than that of HKUST-1, due to reactant diffusion within the polystyrene layer, its suitability for heterogeneous catalysis remains unaffected. Thus, the addition of the polystyrene protective layer does not compromise the catalytic efficacy of HKUST-1. The practicality of heterogeneous catalysts hinges on their recyclability and reusability. As shown in Figure 7c, the catalytic activity of the HKUST-1@EPP demonstrates a negligible decline upon multiple reuses (initial: 90.3%, sixth: 83.6%), with a slight fluctuation likely stemming from experimental variability. The SEM image and the PXRD pattern of the HKUST-1@EPP remain the same, confirming the desirable stability of HKUST-1 in the composite (Figures S5 and S6). These findings collectively indicate the promising performance and practical utility of HKUST-1@EPP in heterogeneous catalysis.

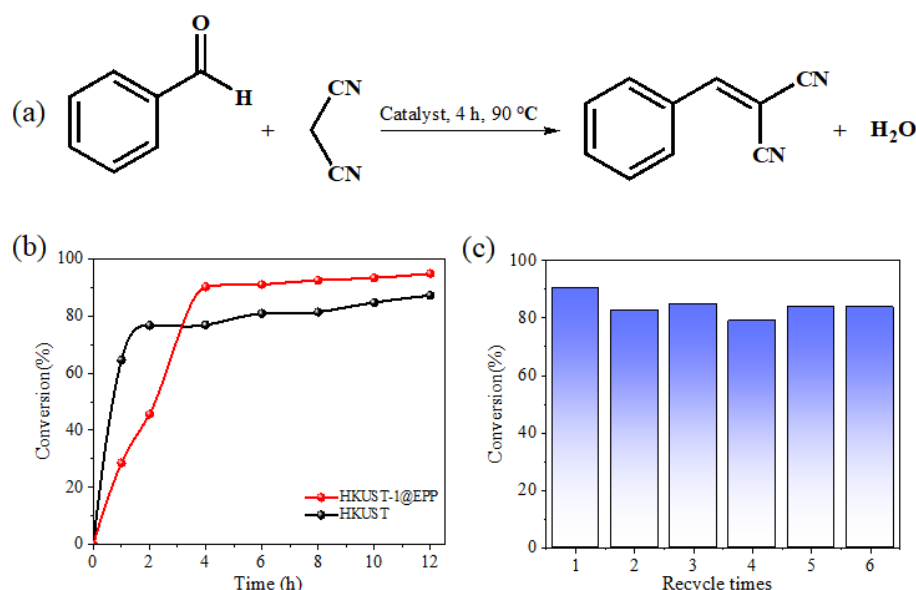


Figure 7. (a) Scheme of Knoevenagel condensation reaction; (b) the catalytic conversion rate of HKUST-1 and HKUST-1@EPP; and (c) recycling experiment of HKUST-1@EPP.

4. Conclusions

This study introduces an economical and straightforward approach to enhance the stability of MOFs through encapsulation with recycled expanded polystyrene plastic waste, known for its desirable stability and hydrophobic nature. The water stability of MOFs@EPP is markedly improved, owing to the hydrophobic polystyrenes. This method can be widely applied to different moisture-sensitive MOFs, such as HKUST-1, MOF-74(Zn), and MIL-53(Al). Notably, HKUST-1@EPP exhibits enduring stability during prolonged water immersion (even for 30 days) and Knoevenagel condensation reactions containing water, demonstrating a commendable catalytic performance and cyclic activity. This method offers a promising solution for enhancing MOFs with limited moisture stability while simultaneously addressing the issue of white pollution stemming from plastic waste.

Supplementary Materials: The following supporting information can be downloaded at: <https://www.mdpi.com/article/10.3390/pr12050961/s1>, Figure S1: Pore size distribution of HKUST-1 nanoparticles; Figure S2: Pore size distribution of HKUST-1@EPP; Figure S3: XRD pattern of MOF-74(Zn) nanoparticles; Figure S4: XRD pattern of MIL-53(Al) nanoparticles. Figure S5: SEM image of HKUST-1@EPP after the reaction; Figure S6: XRD pattern of HKUST-1@EPP after the reaction; Figure S7: SEM image of HKUST-1 nanoparticles after the reaction.

Author Contributions: Conceptualization, J.H.; methodology, S.E.H.; formal analysis, R.Y. and D.S.; investigation, R.Y., E.S. and C.L.; data curation, R.Y. and E.S.; writing—original draft preparation, C.L.; writing—review and editing, R.Y.; visualization, D.S.; supervision, J.H.; project administration, J.H. and S.E.H. All authors have read and agreed to the published version of the manuscript.

Funding: This research was funded by the National Natural Science Foundation of China (Grant No: 22178090), the Hunan Provincial Natural Science Fund for Excellent Young Scholars (2020JJ3002), the Open Fund from Hunan Provincial Key Laboratory of Advanced Materials for New Energy Storage and Conversion (Grant No: 2018TP1037-201902), and the Hunan University Training Program for Excellent Young Scholars.

Data Availability Statement: The data that support the presented results of this study are available from the corresponding author upon reasonable request.

Conflicts of Interest: The authors declare no conflicts of interest.

References

1. Zhi, X.; Bairoliya, S.; Cho, Z.; Cao, B. Plastic-microbe interaction in the marine environment: Research methods and opportunities. *Environ. Int.* **2023**, *171*, 107716.
2. Poto, M.; Elvevoll, E.; Sundset, M.; Eilertsen, K.; Morel, M.; Jensen, I. Suggestions for a systematic regulatory approach to ocean plastics. *Foods* **2021**, *10*, 2197. [CrossRef] [PubMed]
3. Vlaanderen, E.; Ghaly, T.; Moore, L.; Focardi, A.; Paulsen, I.; Tetu, S. Plastic leachate exposure drives antibiotic resistance and virulence in marine bacterial communities. *Environ. Pollut.* **2023**, *327*, 121558. [CrossRef]
4. Fonseca, W.; Meng, X.; Deng, D. Trash to treasure: Transforming waste polystyrene cups into negative electrode materials for sodium ion batteries. *ACS Sustain. Chem. Eng.* **2015**, *3*, 2153–2159. [CrossRef]
5. Hopewell, J.; Dvorak, R.; Kosior, E. Plastics recycling: Challenges and opportunities. *Philos. Trans. R. Soc. B Biol. Sci.* **2009**, *364*, 2115–2126. [CrossRef]
6. Yansaneh, O.; Zein, S. Latest advances in waste plastic pyrolytic catalysis. *Processes* **2022**, *10*, 683. [CrossRef]
7. Brems, A.; Baeyens, J.; Dewil, R. Recycling and recovery of post-consumer plastic solid waste in a European context. *Therm. Sci.* **2012**, *16*, 669–685. [CrossRef]
8. Thu, H.; Ngoc, M.; Thang, V.; Nguyen, H.; Van-Tien, B. Water transferable, customizable highly ordered honeycomb film from polystyrene foam waste for complex surface patterning in confined space. *J. Appl. Polym. Sci.* **2024**, *141*, e55241.
9. Suellen, S.; Felipe, L.; Esperidian, A.; Hélio, W. Recycling expanded polystyrene with a biodegradable solvent to manufacture 3D printed prototypes and finishing materials for construction. *J. Polym. Environ.* **2022**, *30*, 3701–3717.
10. Luo, X.; Zhan, J.; Mei, Q.; Zhang, S. Selective oxidative upgrade of waste polystyrene plastics by nitric acid to produce benzoic acid. *Green Chem.* **2023**, *25*, 6717–6727. [CrossRef]
11. Albert, O.; Jerald, Y.; Feng, Z.; Tristan, T.; Jason, Y. Organocatalytic aerobic oxidative degradation of polystyrene to aromatic acids. *ACS Sustain. Chem. Eng.* **2023**, *11*, 12514–12522.
12. Ribeiro, M.; Pinto, R.; Silva, R.; Vieira, C. Sulfonated expanded polystyrene waste promotes the (+)-citronellal cyclization reaction: A sustainable alternative process for biomass valorization. *Waste Biomass Valor.* **2021**, *12*, 4695–4702. [CrossRef]
13. Jin, P.; Tan, W.; Huo, J.; Liu, T.; Liang, Y.; Wang, S.; Bradshaw, D. Hierarchically porous MOF/polymer composites via interfacial nanoassembly and emulsion polymerization. *J. Mater. Chem. A* **2018**, *6*, 20473–20479. [CrossRef]
14. Chen, L.; Ding, X.; Huo, J.; El Hankari, S.; Bradshaw, D. Facile synthesis of magnetic macroporous polymer/MOF composites as separable catalysts. *J. Mater. Sci.* **2018**, *54*, 370–3829. [CrossRef]
15. Huo, J.; Marcello, M.; Garai, A.; Bradshaw, D. MOF-polymer composite microcapsules derived from Pickering emulsions. *Adv. Mater.* **2013**, *25*, 2717–2722. [CrossRef] [PubMed]
16. Wang, K.; Li, Y.; Xie, L.; Li, X.; Li, J. Construction and application of base-stable MOFs: A critical review. *Chem. Soc. Rev.* **2022**, *51*, 6417–6441. [CrossRef] [PubMed]
17. Song, D.; Hu, C.; Gao, Z.; Yang, B.; Li, Q.; Zhan, X.; Tong, X.; Tian, J. Metal-organic frameworks (MOFs) derived materials used in Zn-air battery. *Materials* **2022**, *15*, 5837. [CrossRef]
18. Jaffar, Z.; Yunus, N.; Shaharun, M.; Allim, M.; Rahim, A. Incorporated metal-organic framework hybrid materials for gas separation, catalysis and wastewater treatment. *Processes* **2022**, *10*, 2368. [CrossRef]
19. Ding, M.; Cai, X.; Jiang, H. Improving MOF stability: Approaches and applications. *Chem. Sci.* **2019**, *10*, 10209–10230. [CrossRef]

20. Xu, T.; Wang, Y.; Xue, Y.; Li, J.; Wang, Y. MXenes@metal-organic framework hybrids for energy storage and electrocatalytic application: Insights into recent advances. *Chem. Eng. J.* **2023**, *470*, 144247. [\[CrossRef\]](#)
21. Zhang, Y.; Chang, C. Metal-organic framework thin films: Fabrication, modification, and patterning. *Processes* **2020**, *8*, 377. [\[CrossRef\]](#)
22. Zhang, T.; Lin, W. Metal-organic frameworks for artificial photosynthesis and photocatalysis. *Chem. Soc. Rev.* **2014**, *43*, 5982–5993. [\[CrossRef\]](#)
23. Xia, W.; Mahmood, A.; Zou, R.; Xu, Q. Metal-organic frameworks and their derived nanostructures for electrochemical energy storage and conversion. *Energy Environ. Sci.* **2015**, *8*, 1837–1866. [\[CrossRef\]](#)
24. Zhang, Z.; Yao, Z.; Xiang, S.; Chen, B. Perspective of microporous metal-organic frameworks for CO₂ capture and separation. *Energy Environ. Sci.* **2014**, *7*, 2868–2899. [\[CrossRef\]](#)
25. Qiu, S.; Xue, M.; Zhu, G. Metal-organic framework membranes: From synthesis to separation application. *Chem. Soc. Rev.* **2014**, *43*, 6116–6140. [\[CrossRef\]](#) [\[PubMed\]](#)
26. Zhao, M.; Ou, S.; Wu, C. Porous metal-organic frameworks for heterogeneous biomimetic catalysis. *Acc. Chem. Res.* **2014**, *47*, 1199–1207. [\[CrossRef\]](#)
27. Gascon, J.; Corma, A.; Kapteijn, F.; Llabrés, F. Metal-organic framework catalysis: Quo vadis? *ACS Catal.* **2013**, *4*, 361–378. [\[CrossRef\]](#)
28. Bair, J.; Schramm, Y.; Sergeev, A.; Clot, E.; Eisenstein, O.; Hartwig, J. Linear-selective hydroarylation of unactivated terminal and internal olefins with trifluoromethyl-substituted arenes. *J. Am. Chem. Soc.* **2014**, *136*, 13098–13101. [\[CrossRef\]](#) [\[PubMed\]](#)
29. Ahmed, I.; Jhung, S. Composites of metal-organic frameworks: Preparation and application in adsorption. *Mater. Today* **2014**, *17*, 136–146. [\[CrossRef\]](#)
30. Chen, Z.; Kent, O.; Le, O. Rational design of stable functional metal-organic frameworks. *Mater. Today* **2023**, *10*, 3257–3268. [\[CrossRef\]](#)
31. Hung, P.; Lin, P.; Wang, X.; Ho, J.-a.A. Metal-organic frameworks in diagnostics, therapeutics, and other biomedical applications. *J. Chin. Chem. Soc.* **2023**, *70*, 1284–1296. [\[CrossRef\]](#)
32. Yang, S.; Peng, L.; Sun, D.; Asgari, M.; Oveisi, E.; Trukhina, O.; Bulut, S.; Jamali, A.; Queen, W. A new post-synthetic polymerization strategy makes metal-organic frameworks more stable. *Chem. Sci.* **2019**, *10*, 4542–4549. [\[CrossRef\]](#) [\[PubMed\]](#)
33. Li, R.; Wang, Z.; Yuan, Z.; Van Horne, C.; Freger, V.; Lin, M.; Cai, R.; Chen, J. A comprehensive review on water stable metal-organic frameworks for large-scale preparation and applications in water quality management based on surveys made since 2015. *Crit. Rev. Env. Sci. Technol.* **2022**, *52*, 4038–4071. [\[CrossRef\]](#)
34. Zhang, J.; Zhang, H.; Du, Z.; Wang, X.; Yu, S.; Jiang, H. Water-stable metal-organic frameworks with intrinsic peroxidase-like catalytic activity as a colorimetric biosensing platform. *Chem. Commun.* **2014**, *50*, 1092–1094. [\[CrossRef\]](#) [\[PubMed\]](#)
35. Burtch, N.; Jasuja, H.; Walton, K. Water stability and adsorption in metal-organic frameworks. *Chem. Rev.* **2014**, *114*, 10575–10612. [\[CrossRef\]](#)
36. Canivet, J.; Fateeva, A.; Guo, Y.; Coasne, B.; Farrusseng, D. Water adsorption in MOFs: Fundamentals and applications. *Chem. Soc. Rev.* **2014**, *43*, 5594–5617. [\[CrossRef\]](#)
37. Mukherjee, S.; Kansara, A.; Saha, D.; Gonnade, R.; Mullangi, D.; Manna, B.; Desai, A.; Thorat, S.; Singh, P.; Mukherjee, A.; et al. An ultrahydrophobic fluorinated metal-organic framework derived recyclable composite as a promising platform to tackle marine oil spills. *Chem. Eur. J.* **2016**, *22*, 10937–10943. [\[CrossRef\]](#)
38. Nguyen, J.; Cohen, S. Moisture-resistant and superhydrophobic metal-organic frameworks obtained via postsynthetic modification. *J. Am. Chem. Soc.* **2010**, *132*, 4560–4561. [\[CrossRef\]](#) [\[PubMed\]](#)
39. Sun, Q.; He, H.; Gao, W.; Aguila, B.; Wojtas, L.; Dai, Z.; Li, J.; Chen, Y.; Xiao, F.; Ma, S. Imparting amphiphobicity on single-crystalline porous materials. *Nat. Commun.* **2016**, *7*, 13300. [\[CrossRef\]](#)
40. Deng, X.; Zheng, S.; Zhong, Y.; Hu, J.; Chung, L.; He, J. Conductive MOFs based on thiol-functionalized linkers: Challenges, opportunities, and recent advances. *Coord. Chem. Rev.* **2022**, *450*, 214235. [\[CrossRef\]](#)
41. Spiegel, S.; Wagner, I.; Begum, S.; Schwotzer, M.; Wessely, I.; Braese, S.; Tsotsalas, M. Dynamic surface modification of metal-organic framework nanoparticles via alkoxyamine functional groups. *Langmuir* **2022**, *10*, 6531–6538. [\[CrossRef\]](#) [\[PubMed\]](#)
42. Huang, G.; Yang, Q.; Xu, Q.; Yu, S.; Jiang, H. Polydimethylsiloxane coating for a palladium/MOF composite: Highly improved catalytic performance by surface hydrophobization. *Angew. Chem. Int. Ed.* **2016**, *55*, 7379–7383. [\[CrossRef\]](#) [\[PubMed\]](#)
43. Wee, L.; Lohe, M.; Janssens, N.; Kaskel, S.; Martens, J. Fine tuning of the metal-organic framework Cu₃(BTC)₂ HKUST-1 crystal size in the 100 nm to 5 micron range. *J. Mater. Chem.* **2012**, *22*, 13742–13746. [\[CrossRef\]](#)
44. Vinu, A.; Ariga, K.; Mori, T.; Nakanishi, T.; Hishita, S.; Golberg, D.; Bando, Y. Preparation and characterization of well-ordered hexagonal mesoporous carbon nitride. *Adv. Mater.* **2005**, *17*, 1648–1652. [\[CrossRef\]](#)
45. Ploychompoo, S.; Liang, Q.; Zhou, X.; Wei, C.; Luo, H. Fabrication of Zn-MOF-74/polyacrylamide coated with reduced graphene oxide (Zn-MOF-74/rGO/PAM) for As(III) removal. *Phys. E Low-Dimens. Syst. Nanostruct.* **2021**, *125*, 114377. [\[CrossRef\]](#)
46. Rowsell, J.; Yaghi, O. Effects of functionalization, catenation, and variation of the metal oxide and organic linking units on the low-pressure hydrogen adsorption properties of metal-organic frameworks. *J. Am. Chem. Soc.* **2006**, *128*, 1304–1315. [\[CrossRef\]](#) [\[PubMed\]](#)
47. Wang, Z.; Chen, Q. Conversion of 5-hydroxymethylfurfural into 5-ethoxymethylfurfural and ethyl levulinate catalyzed by MOF-based heteropolyacid materials. *Green Chem.* **2016**, *18*, 5884–5889. [\[CrossRef\]](#)

48. Li, J.; Sun, X.; Subhan, S.; Gong, W.; Li, W.; Sun, W.; Zhang, Y.; Lu, M.; Ji, H.; Zhao, Z.; et al. Construction of novel Cu-based bimetal polycrystal@carbon catalyst prepared from bimetal HKUST-1 type MOFs (MOF-199s) for ultrafast reduction of 4-nitrophenol via interfacial synergistic catalysis. *Chem. Eng. J.* **2022**, *446*, 137314. [[CrossRef](#)]
49. Al-Janabi, N.; Alfutimie, A.; Siperstein, F.; Fan, X. Underlying mechanism of the hydrothermal instability of Cu₃(BTC)₂ metal-organic framework. *Front. Chem. Sci. Eng.* **2016**, *10*, 103–107. [[CrossRef](#)]
50. Majano, G.; Martin, O.; Hammes, M.; Smeets, S.; Baerlocher, C.; Perez-Ramirez, J. Solvent-mediated reconstruction of the metal-organic framework HKUST-1 (Cu₃(BTC)₂). *Adv. Funct. Mater.* **2014**, *24*, 3855–3865. [[CrossRef](#)]
51. Carotenuto, G.; Nicolais, F. Reversible thermochromic nanocomposites based on thiolate-capped silver nanoparticles embedded in amorphous polystyrene. *Materials* **2009**, *2*, 1323–1340. [[CrossRef](#)]
52. Van Beurden, K.; Koning, S.; Molendijk, D.; Schijndel, J. The knoevenagel reaction: A review of the unfinished treasure map to forming carbon-carbon bonds. *Green Chem. Lett. Rev.* **2020**, *13*, 85–100. [[CrossRef](#)]
53. Johari, S.; Johan, M.; Khaligh, N. An overview of metal-free sustainable nitrogen-based catalytic knoevenagel condensation reaction. *Org. Biomol. Chem.* **2022**, *20*, 2164–2186. [[CrossRef](#)] [[PubMed](#)]
54. An, H.; Zhang, J.; Chang, S.; Hou, Y.; Zhu, Q. 2D hybrid architectures constructed from two kinds of polyoxovanadates as efficient heterogeneous catalysts for cyanosilylation and knoevenagel condensation. *Inorg. Chem.* **2020**, *59*, 10578–10590. [[CrossRef](#)] [[PubMed](#)]

Disclaimer/Publisher's Note: The statements, opinions and data contained in all publications are solely those of the individual author(s) and contributor(s) and not of MDPI and/or the editor(s). MDPI and/or the editor(s) disclaim responsibility for any injury to people or property resulting from any ideas, methods, instructions or products referred to in the content.